ICES REPORT 10-47

November 2010

Finite element analysis of the Girkmann problem using the modern *hp*-version and the

by

Antti H. Niemi, Ivo Babuska, Juhani Pitkaranta, Leszek Demkowicz

The Institute for Computational Engineering and Sciences
The University of Texas at Austin
Austin, Texas 78712

Reference: Antti H. Niemi, Ivo Babuska, Juhani Pitkaranta, Leszek Demkowicz, "Finite element analysis of the Girkmann problem using the modern hp-version and the classical h-version", ICES REPORT 10-47, The Institute for Computational Engineering and Sciences, The University of Texas at Austin, November 2010.

Finite element analysis of the Girkmann problem using the modern *hp*-version and the classical *h*-version

Antti H. Niemi[*], Ivo Babuška[†], Juhani Pitkäranta[‡], Leszek Demkowicz[§]

Abstract

We perform finite element analysis of the so called Girkmann problem in structural mechanics. The problem involves an axially symmetric spherical shell stiffened with a foot ring and is approached (i) by using the axisymmetric formulation of linear elasticity theory and (ii) by using a dimensionally reduced shell-ring model. In the first approach the problem is solved with a fully automatic *hp*-adaptive finite element solver whereas the classical *h*-version of the finite element method is used in the second approach. We study the convergence behaviour of the different numerical models and show that accurate stress resultants can be obtained with both models by using effective post-processing formulas.

Keywords: Verification & validation; *hp*-Adaptivity; Shell elements; Post-processing

1 Introduction

In a recent article [1] a challenge was posed to make a computational analysis of a shell problem formulated by Karl Girkmann in his classical textbook [2]. The purpose of this challenge was to find out whether this relatively straightforward engineering problem can be solved routinely and reliably by computers and the existing software of today. The challenge was accepted by various engineers and scientists who addressed the problem but the answers were surprisingly incoherent. In particular the numerical results obtained with the *h*-version of the finite element method had a very large dispersion, see [3, 4] and the Appendix.

The problem of *verification and validation* (V&V), see [5, 6], has come to the forefront of interest because computational science is able to solve large complex problems of engineering. Validation is related to the question whether the exact solution of the mathematical problem (model) describes faithfully the reality so that decisions could be based on the obtained results. Verification is concerned with the question whether the accuracy of the approximate

[*]ICES, University of Texas at Austin, e-mail: ahniemi@ices.utexas.edu
[†]ICES, University of Texas at Austin, e-mail: babuska@ices.utexas.edu
[‡]Department of Mathematics and Systems Analysis, Aalto University, e-mail: juhani.pitkaranta@tkk.fi
[§]ICES, University of Texas at Austin, e-mail: leszek@ices.utexas.edu

solution (for example the finite element solution) is sufficient for the purpose of computation, cf. [7].

A common approach to the verification of numerical methods and computer software is to perform so called *benchmark computations*. The idea is to put the reliability and performance of a computational model into test by solving selected problems whose exact solution is known to a sufficient precision. At the same time, benchmark problems should be difficult enough so that the test is meaningful concerning practical applications of the model. In our opinion, the Girkmann problem serves as a good benchmark problem because the problem description is relatively straightforward, but accurate recovery of the stress resultants has turned out to be a rather non-trivial task.

A detailed finite element analysis of the problem using the p-version has been carried out in [4]. In the present paper a similar analysis is performed using the hp-version in *self-adaptive* manner. Within this approach the analyst's work is limited to specifying the initial geometry while the automatic procedure generates a sequence of finite element meshes with optimal distributions of the element sizes h and the approximation orders p with respect to the degrees of freedom. The advantages of the hp-version of the finite element method in context of thin-walled structures have been demonstrated earlier by Tews and Rachowicz in [8].

Our computations show that the hp-method is successful also in the Girkmann problem especially when the extraction procedure introduced in [9] is used to post-process the stress resultants. The computations were performed using the standard, energy-based version of the hp-adaptive algorithm as described in [10]. The existing software package was modified slightly to incorporate the axisymmetric formulation of linear elasticity theory and the post-processing formulas of the stress resultants.

Motivated by the scattered results of the h-version shell elements reported in [4], we have also solved the problem by using a dimensionally reduced shell-ring model. Such a simplified model was in fact applied to solve and analyze the problem in the original treatment of Girkmann and subsequently in [11]. We rely here on a semi-analytic approach where the kinematic assumptions are first imposed on the continuous level and the resulting dimensionally reduced problem is then solved approximately by using the h-version of the finite element method. More precisely, a classical Reissner-Mindlin type assumption is used on the shell whereas the ring cross section is assumed to remain undeformed. These physical assumptions are then imposed as an Ansatz within the otherwise standard principle of minimum potential energy. The model, first derived in [11], differs slightly from the original one proposed by Girkmann and has turned out to be very accurate as compared with the elasticity theory.

It should be noted that our numerical approach to the dimensionally reduced shell-ring model does *not* involve approximation of the initial shell geometry in contrast to many low-order shell element formulations of commercial finite element codes. In fact, it has been shown in [12, 13] that crude approximation of the shell geometry may deteriorate the accuracy of finite elements if the shell deformation involves strong boundary or interior layers. In the Girkmann problem a dominant boundary layer appears indeed near the junction

between the shell and the ring. It is possible that the error amplification effects associated to the layer approximation are partly responsible of the erroneous results obtained earlier with the h-version shell elements. Another potential source of numerical problems is the transition from shell elements to solid elements at the junction. Either way, our study shows that relatively accurate stress resultants can be computed by using the h-version of the finite element method within a *geometrically compatible* shell-ring model. By utilizing a priori knowledge of the boundary layer, the problem can be solved rather economically on a piecewise uniform (Shishkin) mesh – in particular if selective under-integration is applied to circumvent transverse shear locking.

The paper is organized as follows. The Girkmann problem statement is recalled in Section 2 and the two different mathematical models are formulated in Section 3. The finite element approaches for both models are then described in Section 4 and the results of computation are shown in Section 5. A summary of our results is presented in Section 6 whereas the earlier results can be found from the Appendix.

2 The Girkmann problem statement

A spherical dome made of reinforced concrete, assumed to be homogeneous, isotropic and linearly elastic with Young's modulus $E = 20.59\,\mathrm{GPa}$ and Poisson's ratio $\nu = 0$ is connected to a stiffening ring at the meridional angle $\alpha = 40°$ as shown in Fig. 1. The crown radius, i.e. the distance from the axis of rotational symmetry to the midpoint of the junction between the spherical shell and the stiffening ring, is $\rho_0 = 15.00\,\mathrm{m}$. The thickness of the shell is $d = 0.06\,\mathrm{m}$ so that the slenderness ratio is $t = d/r_0 = 2.57 \cdot 10^{-3}$ where $r_0 = \rho_0/\sin\alpha = 23.34\,\mathrm{m}$ is the radius of the midsurface of the shell. The dimensions of the stiffening ring are $a = 0.60\,\mathrm{m}$ and $b = 0.50\,\mathrm{m}$.

We follow the original problem statement where the ring is assumed to be weightless while a gravity load of magnitude $F = 32690\,\mathrm{N/m^3}$ acts on the shell roof. The gravity of the dome is then equilibrated by a uniform normal pressure $p = 27256\,\mathrm{Pa}$ acting at the base AB of the ring. The quantities of interest are:

1. The shear force Q and the bending moment M acting at the junction between the spherical shell and the stiffening ring.

2. The location (meridional angle) and the magnitude of the maximum bending moment in the shell.

The Girkmann problem, as stated above, is considered as a benchmark problem for evaluating verification procedures of numerical methods in structural mechanics. This standpoint was strengthened in the problem statement of [1] by urging analysts to

1. Verify that their results are accurate to within 5 percent.

2. Describe what kind of numerical model and software were used and how the accuracy of the data was verified.

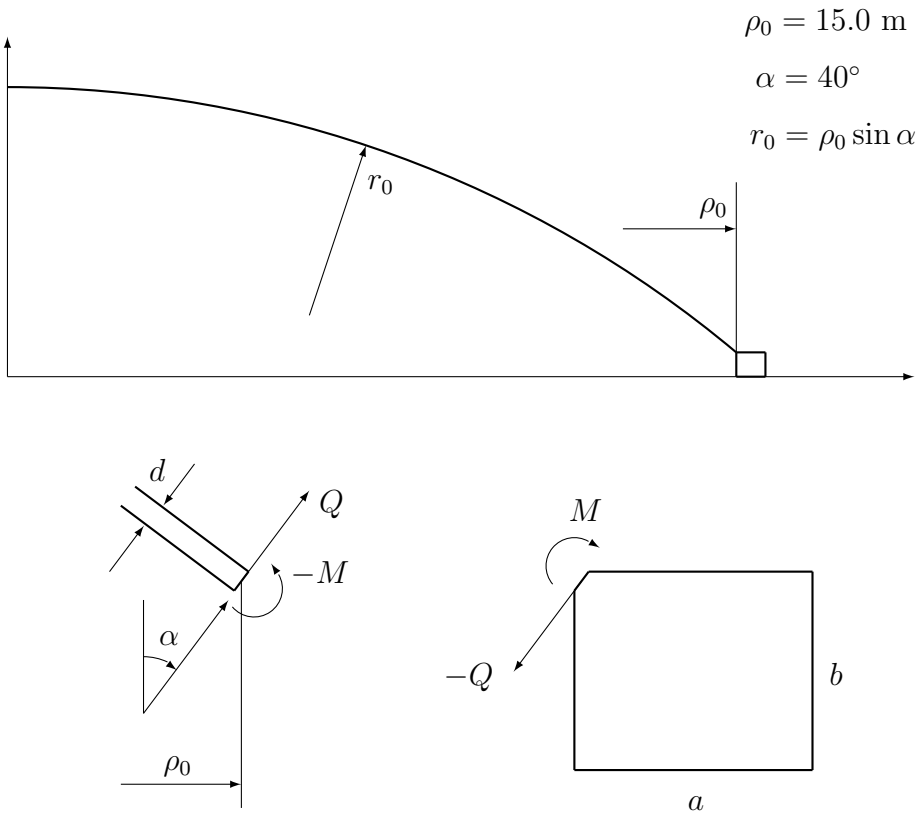

Figure 1: The Girkmann problem. Cross-section of the structure.

3 Mathematical models

Our starting point is the displacement formulation of linear elasticity theory for a body occupying a region Ω. The formulation is based on the variational principle of virtual work equivalent to the principle of minimum potential energy: Find the displacement field $\mathbf{u}$ in the energy space $\mathcal{U}(\Omega)$ such that

$$\mathcal{A}(\mathbf{u}, \mathbf{v}) = \mathcal{L}(\mathbf{v}) \text{ for all } \mathbf{v} \in \mathcal{U}(\Omega)$$

Here $\mathcal{A}(\mathbf{u}, \mathbf{v})$ is the energy product (virtual work of internal stresses) defined in terms of the stress tensor $\boldsymbol{\sigma}$ and the strain tensor $\boldsymbol{\varepsilon}$ as

$$\mathcal{A}(\mathbf{u}, \mathbf{v}) = \int_\Omega \boldsymbol{\sigma}(\mathbf{u}) : \boldsymbol{\varepsilon}(\mathbf{v}) \, \mathrm{d}\Omega$$

and $\mathcal{L}(\mathbf{v})$ is the load functional (virtual work of external stresses) defined as

$$\mathcal{L}(\mathbf{v}) = \int_\Omega \mathbf{f} \cdot \mathbf{v} \, \mathrm{d}\Omega + \int_\Gamma \mathbf{g} \cdot \mathbf{v} \, \mathrm{d}\Gamma$$

The terms $\mathbf{f}$ and $\mathbf{g}$ represent the volume load on Ω and the surface traction on the boundary $\Gamma = \partial\Omega$, respectively. The energy space $\mathcal{U}(\Omega)$ is defined as

$$\mathcal{U}(\Omega) = \{\mathbf{u} \mid \mathcal{A}(\mathbf{u}, \mathbf{u}) < \infty\}$$

and is associated with the energy norm

$$|\!|\!| \mathbf{u} |\!|\!| = \sqrt{\mathcal{A}(\mathbf{u}, \mathbf{u})}. \tag{1}$$

3.1 Axisymmetric solid model

Because the domain, the material properties and the external loads are axially symmetric in the Girkmann problem, the computational domain Ω may be defined as the cross section of the structure (Fig. 1). The problem can then be formulated in terms of the cylindrical coordinates ρ, φ, z in such way that the solution is independent of the azimuthal angle φ and $\mathrm{d}\Omega = \rho \, \mathrm{d}\rho \, \mathrm{d}z$. Denoting the displacement vector field by $\mathbf{u} = (u_\rho, u_z)$, the non-vanishing components of the strain tensor are

$$\epsilon_\rho = \frac{\partial u_\rho}{\partial \rho}, \quad \epsilon_\varphi = \frac{u_\rho}{\rho}, \quad \epsilon_z = \frac{\partial u_z}{\partial z}, \quad \epsilon_{\rho z} = \frac{1}{2}\left(\frac{\partial u_\rho}{\partial z} + \frac{\partial u_z}{\partial \rho}\right)$$

and we have

$$\boldsymbol{\sigma} : \boldsymbol{\varepsilon} = \sigma_\rho \epsilon_\rho + \sigma_z \epsilon_z + \sigma_\varphi \epsilon_\varphi + 2\sigma_{\rho z} \epsilon_{\rho z}$$

Notice that the azimuthal strain ϵ_φ accounts for the true, three-dimensional nature of the problem in spite of the fact that we have only two independent variables ρ and z.

Since the Poisson ratio ν is vanishing, the stress and the strain tensor are related by the simple law $\boldsymbol{\sigma} = E\boldsymbol{\varepsilon}$. Moreover, square-integrability of ϵ_φ requires the enforcement of the symmetry condition $u_\rho = 0$ at $\rho = 0$. Concerning the external loads $\mathbf{f} = (f_\rho, f_z)$ and $\mathbf{g} = (g_\rho, g_z)$, we set

$$\mathbf{f} = \begin{cases} (0, -F) & \text{on the shell domain } \Omega_S \subset \Omega \\ (0, 0) & \text{on the ring domain } \Omega_R \subset \Omega \end{cases}$$

$$\mathbf{g} = \begin{cases} (0, p) & \text{on } \Gamma_{AB} \\ (0, 0) & \text{on } \Gamma \setminus \Gamma_{AB} \end{cases}$$

in accordance with the problem statement. This completes the mathematical formulation of the Girkmann problem as an axisymmetric problem of linear elasticity theory.

3.2 Axisymmetric shell-ring model

The above two-dimensional problem may be simplified further by restricting the energy space $\mathcal{U}(\Omega)$ by using appropriate kinematic assumptions. It is advantageous to use different assumptions for the shell domain Ω_S and the ring domain Ω_R so that the energy product and the load functional are split formally as

$$\mathcal{A}(\mathbf{u}, \mathbf{v}) = \mathcal{A}_S(\mathbf{u}, \mathbf{v}) + \mathcal{A}_R(\mathbf{u}, \mathbf{v}), \quad \mathcal{L}(\mathbf{v}) = \mathcal{L}_S(\mathbf{v}) + \mathcal{L}_R(\mathbf{v})$$

with the continuity of the displacement field being enforced at the junction $\Omega_S \cap \Omega_R$.

The simplification begins with parametrization of the shell domain Ω_S by using the spherical coordinates r, θ, φ (radial, polar, azimuthal). Denoting the corresponding displacement by $\mathbf{u} = (u_\theta, u_r)$, the non-vanishing components of the strain tensor take the form

$$\epsilon_\theta = \frac{1}{r}\frac{\partial u_\theta}{\partial \theta} + \frac{\partial u_r}{r}, \quad \epsilon_r = \frac{\partial u_r}{r}, \quad \epsilon_\varphi = \frac{1}{r}(u_\theta \cot\theta + u_r), \quad \epsilon_{r\theta} = \frac{1}{2}\left(\frac{\partial u_\theta}{\partial r} + \frac{1}{r}\frac{\partial u_r}{\partial \theta} - \frac{u_\theta}{r}\right) \tag{2}$$

The displacement field is then restricted in accordance with the lowest-order shell theory as

$$u_\theta(r, \theta) = u(\theta) + (r - r_0)\psi(\theta), \quad u_r(r, \theta) = w(\theta), \quad 0 \le \theta \le \alpha \tag{3}$$

so that material fibres perpendicular to the shell midsurface before deformation are assumed to remain straight and unstretched after the deformation.

The strains (2) may now be expanded as

$$\epsilon_\theta = \frac{1}{r}[\beta_\theta + (r - r_0)\kappa_\theta], \quad \epsilon_\varphi = \frac{1}{r}[\beta_\varphi + (r - r_0)\kappa_\varphi], \quad \epsilon_{r\theta} = \frac{1}{2r}\rho_\theta$$

where

$$\begin{aligned} &\beta_\theta = u' + w, \quad \beta_\varphi = u\cot\theta + w \\ &\rho_\theta = r_0\psi + w' - u \\ &\kappa_\theta = \psi', \quad \kappa_\varphi = \psi\cot\theta \end{aligned}$$

Note that here the geometric curvature of the shell in the azimuthal direction is represented by the strains β_φ, κ_φ. Taking into account that $\mathrm{d}\Omega_s = r^2 \sin\theta \, \mathrm{d}r \, \mathrm{d}\theta$, the shell energy product $\mathcal{A}_S(\mathbf{u}, \mathbf{v})$ may be integrated with respect to r and written in terms of the generalized displacement field $\mathbf{u} = (u, w, \psi)$ as

$$\mathcal{A}_S(\mathbf{u}, \mathbf{v}) = \mathcal{A}_{\boldsymbol{\beta}}(\mathbf{u}, \mathbf{v}) + \mathcal{A}_{\boldsymbol{\rho}}(\mathbf{u}, \mathbf{v}) + \mathcal{A}_{\boldsymbol{\kappa}}(\mathbf{u}, \mathbf{v})$$

where

$$\begin{aligned}
\mathcal{A}_{\boldsymbol{\beta}}(\mathbf{u}, \mathbf{v}) &= Ed \int_0^\alpha [\beta_\theta(\mathbf{u})\beta_\theta(\mathbf{v}) + \beta_\varphi(\mathbf{u})\beta_\varphi(\mathbf{v})] \, \sin\theta \, \mathrm{d}\theta \\
\mathcal{A}_{\boldsymbol{\rho}}(\mathbf{u}, \mathbf{v}) &= \frac{Ed}{2} \int_0^\alpha \rho_\theta(\mathbf{u})\rho_\theta(\mathbf{v}) \, \sin\theta \, \mathrm{d}\theta \\
\mathcal{A}_{\boldsymbol{\kappa}}(\mathbf{u}, \mathbf{v}) &= \frac{Ed^3}{12} \int_0^\alpha [\kappa_\theta(\mathbf{u})\kappa_\theta(\mathbf{v}) + \kappa_\varphi(\mathbf{u})\kappa_\varphi(\mathbf{v})] \, \sin\theta \, \mathrm{d}\theta
\end{aligned}$$

correspond to the virtual work associated with membrane, transverse shear and bending deformations, respectively.

The gravity load is idealized to act on the shell midsurface with the load density $G = Fd$ as in

$$\mathcal{L}_S(\mathbf{u}) = \int_0^\alpha G[\sin\theta \, u(\theta) - \cos\theta \, w(\theta)] \, r_0^2 \sin\theta \, \mathrm{d}\theta$$

Concerning the deformation of the ring, we assume that the motion of the cross section is that of a rigid body written in terms of the cylindrical coordinates ρ, z as

$$u_\rho(\rho, z) = U + \Psi(z - z_0), \quad u_z(\rho, z) = W - \Psi(\rho - \rho_0) \tag{4}$$

Here U and W represents the horizontal and verical translation respectively, and Ψ represents the rotation around the point $P_0 = (\rho_0, z_0)$ taken to be the midpoint of the junction. Accordingly, the only non-vanishing strain component is

$$\epsilon_\varphi = \frac{1}{\rho}(U + \Psi(z - z_0)) \tag{5}$$

The continuity of the displacement fields (4) and (3) at the shell-ring interface implies that

$$\begin{cases}
U = u(\alpha)\cos\alpha + w(\alpha)\sin\alpha \\
W = -u(\alpha)\sin\alpha + w(\alpha)\cos\alpha \\
\Psi = \psi(\alpha)
\end{cases} \tag{6}$$

Upon substituting (6) into (5), the ring energy product may be written in terms of the generalized displacement field $\mathbf{u} = (u, w, \psi)$ as

$$\mathcal{A}_R(\mathbf{u}, \mathbf{v}) = \int_{\Omega_R} \epsilon_\varphi(\mathbf{u})\epsilon_\varphi(\mathbf{v}) \, \rho \, \mathrm{d}\rho\mathrm{d}z \tag{7}$$

and, Eqs. (6) given, the corresponding load functional reads

$$\mathcal{L}_R(\mathbf{v}) = \int_{\rho_A}^{\rho_B} p[W - \Psi(\rho - \rho_0)] \, \rho \, \mathrm{d}\rho \tag{8}$$

4 Computational models

In this section, we describe the finite element procedures used to solve the Girkmann problem. We will utilize a modern *hp*-adaptive mesh-refinement algorithm in context of the axisymmetric solid model and the classical *h*-version in context of the axisymmetric shell-solid model.

4.1 The modern *hp*-version (axisymmetric solid model)

We present here the main idea of the mesh refinement algorithm which is a slightly tweaked version of the general two dimensional *hp*-adaptive algorithm described in [10]. The starting point of the algorithm is a representation of the computational domain $\Omega \subset \mathbb{R}^2$ as a union of triangles and quadrilaterals with possibly curvilinear edges. The initial partitioning, which is constructed using the Geometry Modeling Package (GMP), is supposed to be regular, i.e. the intersection of any two subdomains is either empty, reduces to a single vertex or consists of a whole edge. However, the geometry updates following mesh refinements are allowed to lead to so called one-irregular meshes with constrained, or hanging nodes.

Mesh optimization algorithm

A given coarse *hp*-mesh is refined in both h and p to obtain the corresponding fine mesh. The problem is then solved on the fine mesh and the fine mesh solution $\mathbf{u} = \mathbf{u}_{h/2,p+1}$ is obtained. This is used to determine the optimal mesh hp_{opt} such that the rate of decrease of the error, as measured in the energy norm (1), is maximized:

$$\frac{\|\mathbf{u} - \mathbf{\Pi}_{hp}\mathbf{u}\|^2 - \|\mathbf{u} - \mathbf{\Pi}_{hp_{\text{opt}}}\mathbf{u}\|^2}{N_{hp_{\text{opt}}} - N_{hp}} = \max!$$

Here $\mathbf{\Pi}_{hp}\mathbf{u}$ and $\mathbf{\Pi}_{hp_{\text{opt}}}\mathbf{u}$ denote the projection-based interpolants of the fine grid solution on the original mesh and on the optimal mesh, respectively, while N_{hp} and $N_{hp_{\text{opt}}}$ denote the corresponding numbers of degrees of freedom.

The mesh modifications involving subsections of elements are referred to as *h*-refinements whereas changing the orders of the elements are referred to as *p*-refinements. For quadrilateral elements, the automatic algorithm can perform both type of refinements *anisotropically*, i.e. in the direction of one reference element coordinate only. In our case of axisymmetric formulation of elasticity, this feature is utilized by splitting the energy norm of the error $\mathbf{e} = (e_\rho, e_z)$ over a single element K as

$$\begin{aligned}\|\mathbf{e}\|_K^2 &= \int_K \boldsymbol{\sigma}(\mathbf{e}) : \boldsymbol{\varepsilon}(\mathbf{e})\, \rho \,\mathrm{d}\rho \,\mathrm{d}z \\ &= C_{11} + C_{22} + C_{12}\end{aligned}$$

where the directional error contributions C_{11}, C_{22} and C_{12} are expressed in terms of the

reference element coordinates $\boldsymbol{\xi} = (\xi_1, \xi_2) \in \hat{K}$ as

$$C_{11} = \int_{\hat{K}} \left\{ \left(\frac{\partial e_\rho}{\partial \xi_1} \frac{\partial \xi_1}{\partial \rho} \right)^2 + \left(\frac{\partial e_z}{\partial \xi_1} \frac{\partial \xi_1}{\partial z} \right)^2 + \frac{1}{2} \left(\frac{\partial e_\rho}{\partial \xi_1} \frac{\partial \xi_1}{\partial z} + \frac{\partial e_z}{\partial \xi_1} \frac{\partial \xi_1}{\partial \rho} \right)^2 \right\} \rho(\boldsymbol{\xi})\, J \, \mathrm{d}\boldsymbol{\xi}$$

$$C_{22} = \int_{\hat{K}} \left\{ \left(\frac{\partial e_\rho}{\partial \xi_2} \frac{\partial \xi_2}{\partial \rho} \right)^2 + \left(\frac{\partial e_z}{\partial \xi_2} \frac{\partial \xi_2}{\partial z} \right)^2 + \frac{1}{2} \left(\frac{\partial e_\rho}{\partial \xi_2} \frac{\partial \xi_2}{\partial z} + \frac{\partial e_z}{\partial \xi_2} \frac{\partial \xi_2}{\partial \rho} \right)^2 \right\} \rho(\boldsymbol{\xi})\, J \, \mathrm{d}\boldsymbol{\xi}$$

$$C_{12} = \int_{\hat{K}} \left\{ 2 \frac{\partial e_\rho}{\partial \xi_1} \frac{\partial \xi_1}{\partial \rho} \frac{\partial e_\rho}{\partial \xi_2} \frac{\partial \xi_2}{\partial \rho} + 2 \frac{\partial e_z}{\partial \xi_1} \frac{\partial \xi_1}{\partial z} \frac{\partial e_z}{\partial \xi_2} \frac{\partial \xi_2}{\partial z} + \left(\frac{e_\rho}{\rho(\boldsymbol{\xi})} \right)^2 \right.$$
$$\left. \left(\frac{\partial e_\rho}{\partial \xi_1} \frac{\partial \xi_1}{\partial z} + \frac{\partial e_z}{\partial \xi_1} \frac{\partial \xi_1}{\partial \rho} \right) \left(\frac{\partial e_\rho}{\partial \xi_2} \frac{\partial \xi_2}{\partial z} + \frac{\partial e_z}{\partial \xi_2} \frac{\partial \xi_2}{\partial \rho} \right) \right\} \rho(\boldsymbol{\xi})\, J \, \mathrm{d}\boldsymbol{\xi}$$

Here J denotes the Jacobian (determinant) of the transformation from the physical coordinates to the master element coordinates.

After the new coarse mesh has been determined, the process is repeated until a stopping criterion is met. As a stopping criterion we use the approximate relative error in the energy norm which is computed by using the fine grid solution:

$$\varepsilon = \frac{\left\| \mathbf{u}_{h/2,p+1} - \mathbf{u}_{hp} \right\|}{\left\| \mathbf{u}_{h/2,p+1} \right\|} \leq \tau$$

Post-processing

Upon denoting

$$g_\rho = \sigma_\rho n_\rho + \sigma_{\rho z} n_z$$
$$g_z = \sigma_{\rho z} n_\rho + \sigma_z n_z$$

the unknown reactions at the junction are given by

$$Q = \frac{1}{\rho_0} \int_{-d/2}^{d/2} \left(g_\rho \sin\alpha + g_z \cos\alpha \right) \, \rho \, \mathrm{d}s \tag{9}$$

and

$$M = -\frac{1}{\rho_0} \int_{-d/2}^{d/2} \left(g_\rho (z - z_0) - g_z (\rho - \rho_0) \right) \, \rho \, \mathrm{d}s \tag{10}$$

Because the computational domain has re-entrant corners at the ends of the junction, the stress fields are strongly singular at those points. This makes numerical integration difficult and there is even no theoretical guarantee on the convergence of the stress resultants if computed directly using the definitions. However, an extraction procedure introduced in [9] can be utilized to overcome this difficulty (see also [4]). The details of the variational approach are as follows.

If $\mathbf{u}$ is the exact displacement field and $\mathbf{w}_Q$ is an extraction function defined on the ring domain Ω_R as

$$\mathbf{w}_Q = (\sin\alpha, \cos\alpha), \quad (\rho, z) \in \Omega_R$$

then application of the principle of virtual work on Ω_R yields

$$\mathcal{A}_R(\mathbf{u}, \mathbf{w}_Q) = \mathcal{L}_R(\mathbf{w}_Q) + \rho_0 Q$$

or

$$Q = \frac{1}{\rho_0} \left(\mathcal{L}_R(\mathbf{w}_Q) - \mathcal{A}_R(\mathbf{u}, \mathbf{w}_Q) \right)$$

The choice

$$\mathbf{w}_M = \left(z - z_0, -(\rho - \rho_0) \right), \quad (\rho, z) \in \Omega_R$$

gives similarly

$$M = \frac{1}{\rho_0} \left(\mathcal{L}_R(\mathbf{w}_M) - \mathcal{A}_R(\mathbf{u}, \mathbf{w}_M) \right)$$

If Q_{hp} and M_{hp} denote the corresponding quantities computed using the finite element solution $\mathbf{u}_{hp}$, i.e.

$$Q_{hp} = \frac{1}{\rho_0} \left(\mathcal{L}_R(\mathbf{w}_Q) - \mathcal{A}_R(\mathbf{u}_{hp}, \mathbf{w}_Q) \right) \tag{11}$$

and

$$M_{hp} = \frac{1}{\rho_0} \left(\mathcal{L}_R(\mathbf{w}_M) - \mathcal{A}_R(\mathbf{u}_{hp}, \mathbf{w}_M) \right) \tag{12}$$

then, Cauchy-Schwarz inequality implies that

$$|Q - Q_{hp}| = \frac{1}{\rho_0} |\mathcal{A}_R(\mathbf{u} - \mathbf{u}_{hp}, \mathbf{w}_Q)| \leq \frac{1}{\rho_0} |\!|\!| \mathbf{u} - \mathbf{u}_{hp} |\!|\!|_{\Omega_R} |\!|\!| \mathbf{w}_Q |\!|\!|_{\Omega_R}$$

and

$$|M - M_{hp}| = \frac{1}{\rho_0} |\mathcal{A}_R(\mathbf{u} - \mathbf{u}_{hp}, \mathbf{w}_M)| \leq \frac{1}{\rho_0} |\!|\!| \mathbf{u} - \mathbf{u}_{hp} |\!|\!|_{\Omega_R} |\!|\!| \mathbf{w}_M |\!|\!|_{\Omega_R}$$

In other words, if the finite element solution $\mathbf{u}_{hp}$ is a good approximation of the exact solution $\mathbf{u}$ in terms of the energy norm, then the extracted values of the quantities of interest should also be good approximations of their exact values. In fact, extension of the extraction functions by zero over the whole domain Ω and utilization of a duality argument shows that actually

$$|Q - Q_{hp}| \leq \frac{1}{\rho_0} |\!|\!| \mathbf{u} - \mathbf{u}_{hp} |\!|\!|_{\Omega} |\!|\!| \tilde{\mathbf{w}}_Q - \tilde{\mathbf{w}}_Q^{hp} |\!|\!|_{\Omega}, \quad |M - M_{hp}| \leq \frac{1}{\rho_0} |\!|\!| \mathbf{u} - \mathbf{u}_{hp} |\!|\!|_{\Omega} |\!|\!| \tilde{\mathbf{w}}_M - \tilde{\mathbf{w}}_M^{hp} |\!|\!|_{\Omega}$$

Here $\tilde{\mathbf{w}_Q}, \tilde{\mathbf{w}_M}$ are (smooth) auxiliary functions determined by the corresponding extraction functions, see [4].

Consequently, in theory, the extraction function approach transforms convergence of the displacement field in the energy norm to convergence of the stress resultants very effectively. The numerical results that follow in Section 5 confirm that this is the case in practice too.

4.2 The classical h-version (axisymmetric shell-ring model)

The formulation of the classical h-version finite element method for the axisymmetric shell-ring model is rather straightforward: Each component of the generalized displacement field $\mathbf{u} = (u, w, \psi)$ in Eq. (3) is assumed to be continuous, piecewise linear polynomial associated to a partition

$$0 = \theta_0 < \theta_1 < \theta_2 < \cdots < \theta_N = \alpha$$

In addition to uniform subdivisions we consider piecewise uniform (Shishkin) meshes. These are based on the division of the interval $[0, \alpha]$ into

$$[0, \alpha - \gamma] \quad \text{and} \quad [\alpha - \gamma, \alpha]$$

where $\gamma = 4 \cdot \lambda$ and $\lambda = 3^{1/4} \cdot \sqrt{d/r_0}$ corresponds to the (angular) length scale of the boundary layer in spherical shells, see [14]. The factor 4 is chosen based on empirical numerical experience. In both subintervals $[0, \alpha - \gamma]$ and $[\alpha - \gamma, \alpha]$ we use equidistant meshes of $N/2 + 1$ points (N is assumed to be even).

It has been shown in [14] that the standard displacement-based variational formulation for the shell layer modes becomes a constrained approximation problem when $t/r_0 << 1$. In case of spherical (elliptic) shells, the constraint which becomes gradually enforced as t/r_0 diminishes is the traditional shear (Kirchoff-Love) constraint

$$\rho_\theta = r_0 \psi + w' - u = 0$$

This causes a harmful shear locking effect in the linear finite element model. As a remedy, we have employed selective under-integration where the shear energy term $\mathcal{A}_{\boldsymbol{\rho}}(\mathbf{u}, \mathbf{v})$ is evaluated numerically using the elementwise midpoint rule instead of the customary two-point Gauss-Legendre rule, cf. [12].

Finally, the stiffness of the ring and the supporting pressure affect the degrees of freedom associated to $\theta_N = \alpha$ through Eqs. (5) – (8). The associated integrals were evaluated numerically essentially exactly.

Post-processing

The quantities of interest can be written in terms of the strains as

$$Q = \frac{Ed}{2r_0} \rho_\theta(\alpha), \quad M = -\frac{Ed^3}{12 r_0} \kappa_\theta(\alpha)$$

Let $\mathbf{w}_h^{(Q)} = (u_h^{(Q)}, w_h^{(Q)}, \psi_h^{(Q)})$ and $\mathbf{w}_h^{(M)} = (u_h^{(M)}, w_h^{(M)}, \psi_h^{(M)})$ be extraction functions from the finite element space such that

$$u_h^{(Q)}(\theta_i) = \psi_h^{(Q)}(\theta_i) = 0 \quad \& \quad u_h^{(M)}(\theta_i) = w_h^{(M)}(\theta_i) = 0, \quad i = 0, \ldots, N-1$$

and

$$w_h^{(Q)}(\alpha) = \frac{1}{r_0 \sin\alpha} \quad \& \quad \psi_h^{(M)}(\alpha) = -\frac{1}{r_0 \sin\alpha}$$

The quantities of interest can then be approximated as

$$Q_h = \mathcal{A}_S(\mathbf{u}_h, \mathbf{w}^Q) - \mathcal{L}_S(\mathbf{w}^Q) \quad \& \quad M_h = \mathcal{A}_S(\mathbf{u}_h, \mathbf{w}^M) - \mathcal{L}_S(\mathbf{w}^M)$$

As pointed out in [4], the extraction procedure is formally identical to the computation of stress resultants from the nodal forces (direct stiffness method).

5 Numerical results

5.1 The modern *hp*-version (axisymmetric solid model)

The initial mesh was constructed using the Geometric Modeling Package (GMP) and consists of eight quadrilaterals and one triangle as shown in Figure 2; The shell is divided uniformly into five isoparametric quadrilaterals and the remaining elements are used to mesh the ring in symmetric fashion. The degree of all elements in the initial mesh was chosen to be three.

Mesh optimization

The final one-irregular *hp*-mesh generated by the automatic algorithm is shown in Figures 3 and 4. In all figures, the colour encoding of the element degree p varies from one (dark blue) to eight (dark purple). Triangular colouring within quadrilateral elements stands for anisotropic polynomial degree (horizontal/vertical) within that element.

The influence of the re-entrant corners at the junction on the final mesh becomes evident in Figure 4. The automatic mesh refinement algorithm reacts to the corner singularities by imposing heavy h-refinements towards the ends of the junction. These h-refinements propagate then also to some parts of the domain where the displacement field is expected to be rather smooth. For instance, in view of the classical kinematic hypotheses of Reissner-Mindlin or Kirchoff-Love, the h-refinements in the normal direction of the shell seem unnecessary away from the junction. Anyway, the effect becomes attenuated farther away from the junction thanks to the one-irregularity of the mesh.

Data of interest

The values of the stress resultants were first computed by substituting the finite element solution $\mathbf{u}_{hp}$ into Eqs. (9) and (10) and computing the integrals numerically. Since the approximative stress fields are generally discontinuous over adjacent elements, the results obtained from different sides of the junction may vary. The results reported in Table 5.1 show that this is indeed the case: The values of the shear force Q have not converged even though the estimated error in the energy norm is 0.001%.

The situation becomes completely different if the extraction formulas (11) and (12) are used to post-process the resultants. The results, which are shown in Table 5.1, are much better as predicted by the theory. The data of interest is displayed here with an additional significant digit to illustrate the rapid convergence. Based on this analysis, the final estimates

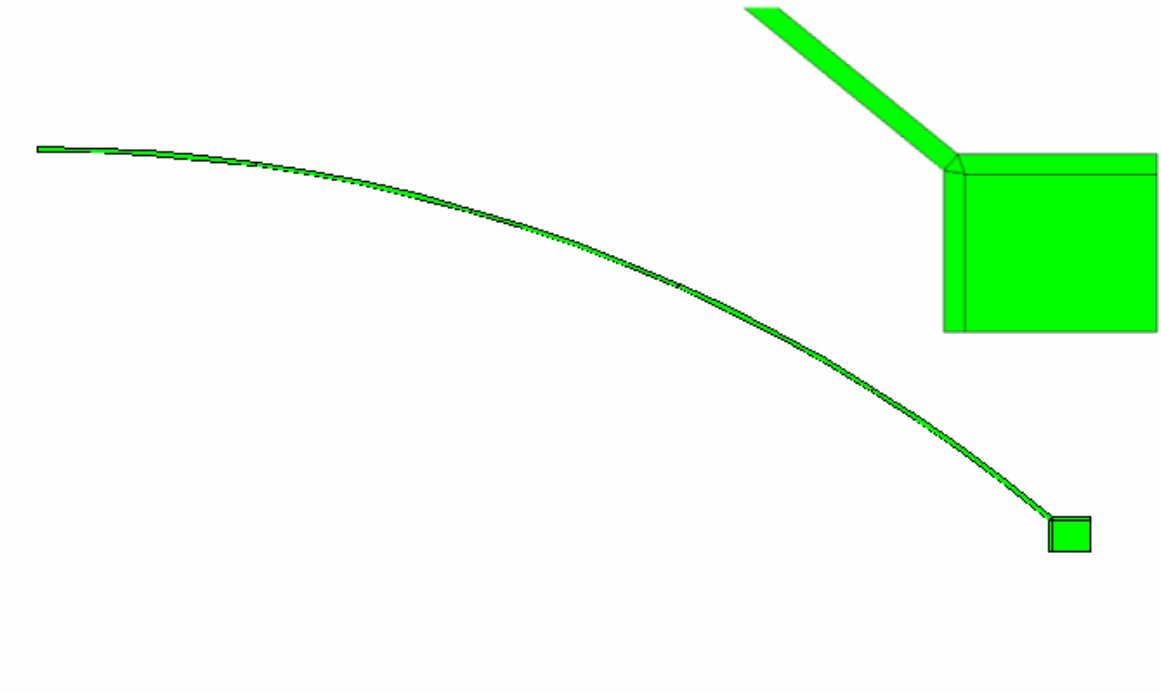

Figure 2: The initial mesh for the *hp*-version (axisymmetric solid model).

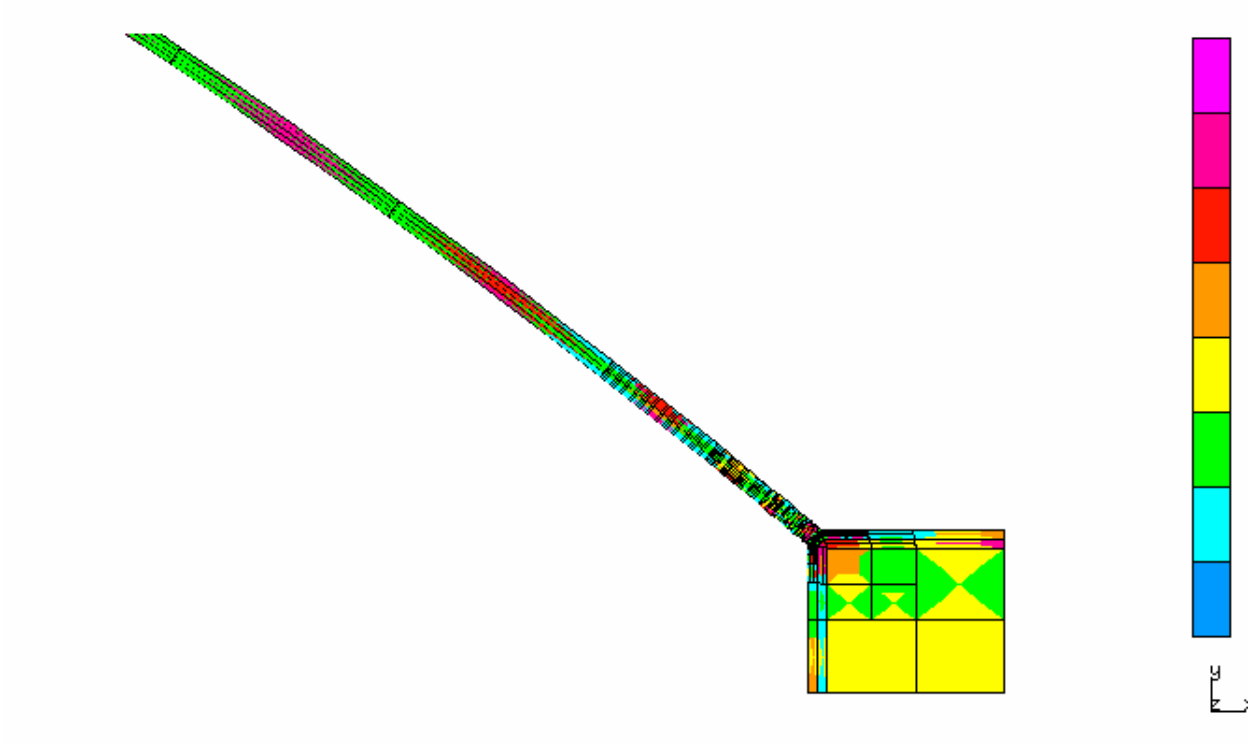

Figure 3: The final *hp*-mesh (axisymmetric solid model).

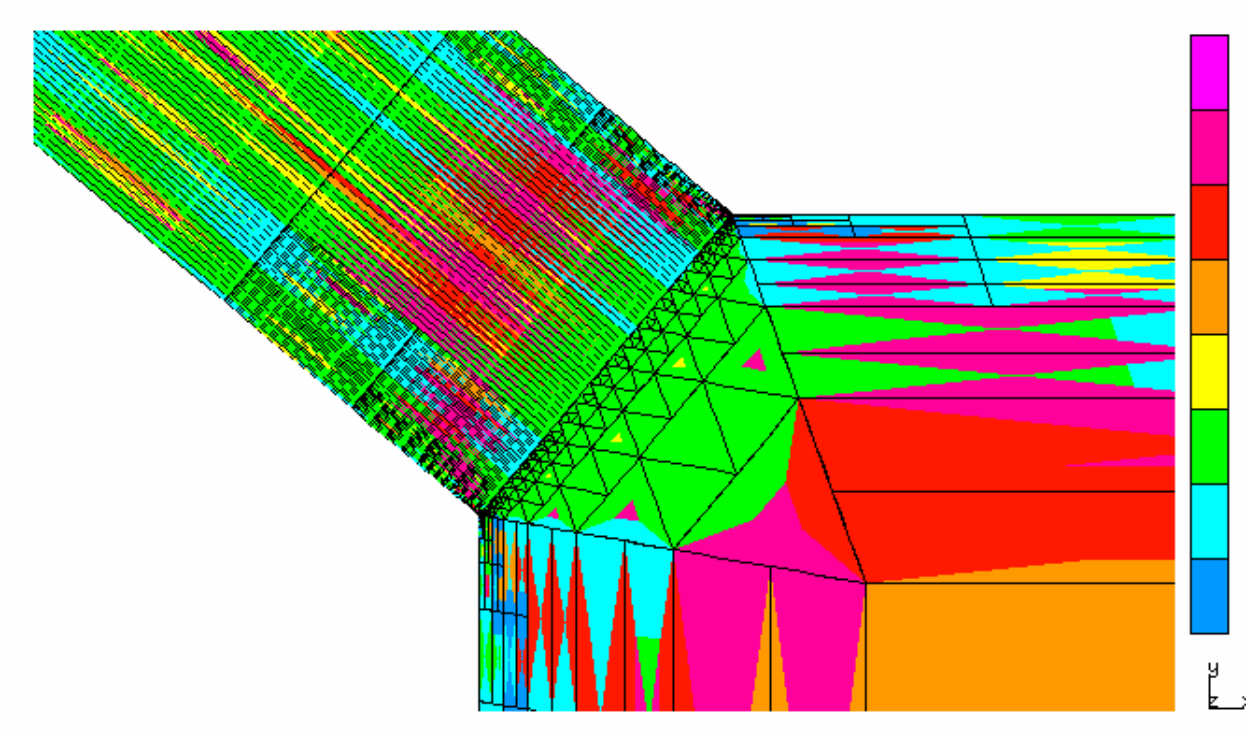

Figure 4: The final *hp*-mesh (axisymmetric solid model). Zoom at the junction.

D.O.F.	Q (N/m) (shell)	Q (N/m) (ring)	M (Nm/m) (shell)	M (Nm/m) (ring)	ε (%)
206	2122.1	244.3	146.27	18.66	4.936
340	1019.0	347.4	-31.81	7.57	0.114
628	1199.2	621.9	-38.38	-11.28	0.056
2272	1123.3	934.7	-40.63	-35.55	0.034
7424	931.2	938.5	-36.08	-36.32	0.013
10292	938.4	946.3	-36.26	-36.85	0.008
13604	932.6	944.1	-36.02	-36.81	0.003
18866	936.5	943.7	-36.78	-36.78	0.001

Table 1: Convergence of the quantities of interest by the *hp*-version (axisymmetric solid model) and direct numerical integration from both sides of the junction (shell/ring).

D.O.F.	Q (N/m)	M (Nm/m)	ε (%)
206	958.72	-38.444	4.936
340	943.81	-37.377	0.114
628	943.73	-37.097	0.056
2272	943.66	-36.849	0.034
7424	943.65	-36.798	0.013
10292	943.65	-36.785	0.008
13604	943.65	-36.790	0.003
18866	943.65	-36.790	0.001

Table 2: Convergence of the quantities of interest computed by the *hp*-version (axisymmetric solid model) and extraction.

for the values of the shear force and bending moment are $Q = 943.65\,\mathrm{N/m}$ and $M = -36.790\,\mathrm{Nm/m}$, respectively.

The location and magnitude of the bending moment can be determined directly by numerical integration because the stress field is smooth away from the junction. The distribution of the bending moment in the shell is shown in Fig. 5. The value and location of the maximum bending moment are estimated to be $M_{\max} = 254.9\,\mathrm{Nm/m}$ and $\theta_{\max} = 38.14°$, respectively.

5.2 The classical *h*-version (axisymmetric shell-ring model)

The results for the *h*-version with and without selective under-integration are shown in Tables 3 and 4. As expected the use of Shishkin-type mesh effectively halves the number of degrees of freedom required to achieve a given accuracy whereas the influence of the reduced integration is even more dramatic.

The results are very close to those obtained with the *hp*-version and, concerning the distribution of the bending moment, a graph identical to 5 is obtained. However, a small difference between the models can be observed near the maxima of the bending moment as Figure 6 shows. The maximum value of the bending moment based on the *h*-version is estimated as $M_{\max} = 254.1\,\mathrm{Nm/m}$ still attained at $\theta_{\max} = 38.14°$.

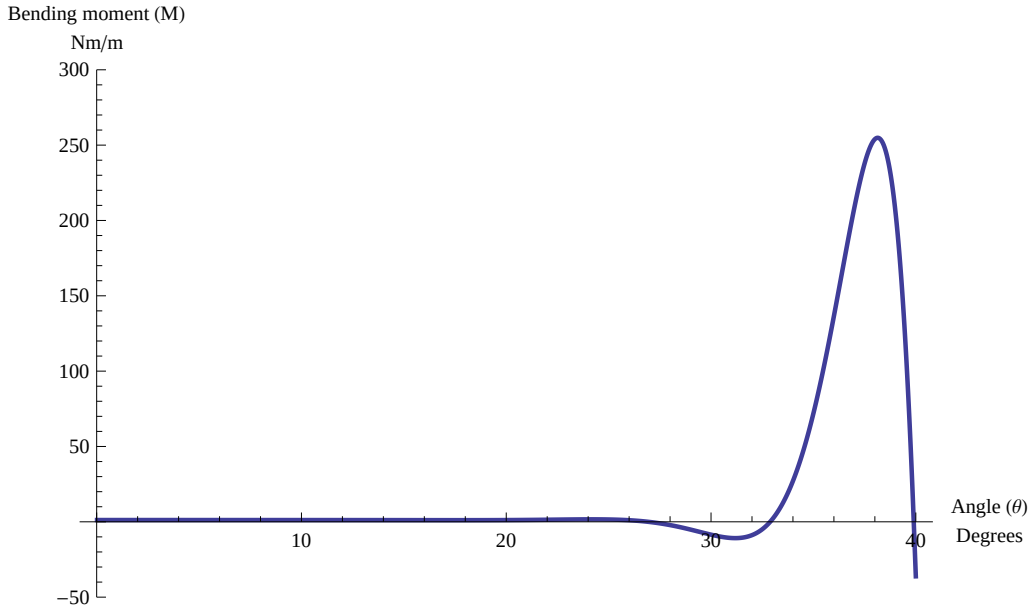

Figure 5: Distribution of the bending moment as computed by the *hp*-version (axisymmetric solid model).

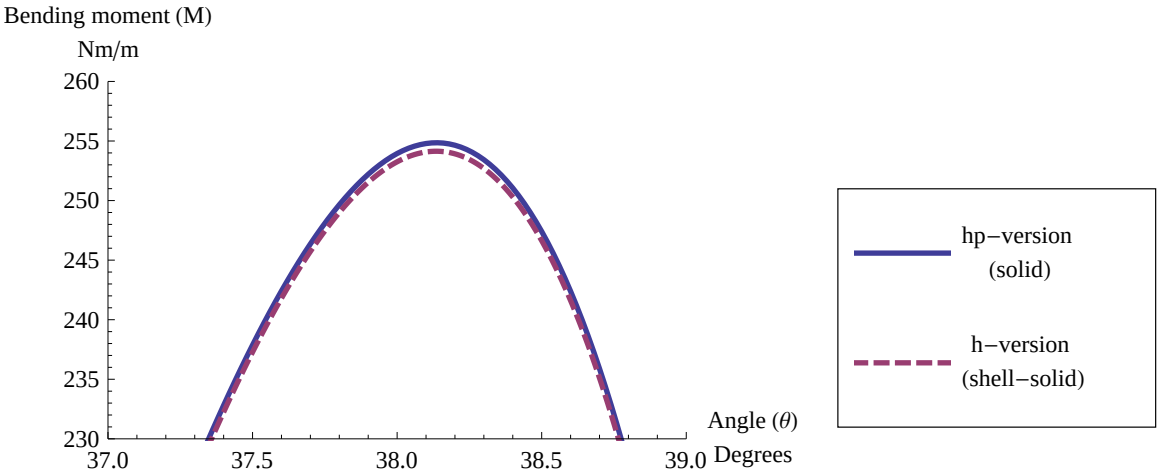

Figure 6: Zoom at the maxima of the bending moment. The *hp*-version (axisymmetric solid model) vs. the *h*-version (axisymmetric shell-solid model).

D.O.F.	Q (N/m) (Shishkin)	Q (N/m) (Uniform)	M (Nm/m) (Shishkin)	M (Nm/m) (Uniform)
51	1004.39	1118.58	-11.95	34.53
99	958.12	988.53	-30.89	-18.44
195	946.31	954.04	-35.74	-32.57
387	943.34	945.28	-36.96	-36.16
771	942.60	943.09	-37.26	-37.06
1539	942.41	942.54	-37.34	-37.29
3075	942.37	942.40	-37.36	-37.34
6147	942.36	942.36	-37.36	-37.36

Table 3: Convergence of the quantities of interest computed by the h-version with selective under-integration (axisymmetric shell-ring model). Uniform vs. piecewise uniform (Shishkin) meshes.

D.O.F.	Q (N/m) (Shishkin)	Q (N/m) (Uniform)	M (Nm/m) (Shishkin)	M (Nm/m) (Uniform)
51	2267.34	2939.45	706.21	1011.10
99	1599.26	2085.71	374.66	623.57
195	1207.38	1491.73	143.84	314.89
387	1027.66	1152.97	23.00	108.52
771	965.91	1007.49	-20.70	8.81
1539	948.42	959.97	-33.08	-24.91
3075	943.88	946.86	-36.29	-34.19
6147	942.74	943.49	-37.09	-36.56
12291	942.45	942.64	-37.30	-37.16
24579	942.38	942.42	-37.35	-37.31

Table 4: Convergence of the quantities of interest computed by the standard h-version (axisymmetric shell-ring model). Uniform vs. piecewise uniform (Shishkin) meshes.

6 Summary

We have presented computational analysis of the Girkmann challenge problem using two different finite element approaches. In the first approach, an automatic *hp*-adaptive finite element solver was applied to the the exact formulation of the problem following axisymmetric linear elasticity theory. In the second approach, the mathematical formulation of the problem was first simplified by using kinematic assumptions and the simplified problem was then solved numerically using the *h*-version of the finite element method.

We have arrived at the following results by applying the *hp*-version for the axisymmetric solid model

- Shear force at the junction: $Q = 943.7\,\mathrm{Nm/m}$
- Bending moment at the junction: $M = -36.79\,\mathrm{Nm/m}$
- Maximum bending moment: $M_{\max} = 254.9\,\mathrm{Nm/m}$
- Location of the maximum bending moment: $\theta_{\max} = 38.14^\circ$

while application of *h*-version to the axisymmetric shell-ring model yield the following results

- Shear force at the junction: $Q = 942.4\,\mathrm{Nm/m}$
- Bending moment at the junction: $M = -37.36\,\mathrm{Nm/m}$
- Maximum bending moment: $M_{\max} = 254.1$
- Location of the maximum bending moment: $\theta_{\max} = 38.14^\circ$

The difference between the results computed with the exact model and with the simplified model is less than two percent.

Model/Element type	Q N	M Nm/m	$\varphi_{\max}$ degrees	$M_{\max}$ Nm/m
Axisymmetric solid (extraction)	943.6	-36.81	38.15	255.10
Axisymmetric solid	940.9	-36.63	38.20	254.92
3D thin solid ($q = 3$)	948.4	-37.31	38.20	254.50
Axisymmetric solid	940.9	-36.80	38.15	254.80

Table 5: Summary of the challenge problem results with the p-version. The term $q = 3$ refers to fixed polynomial degree in the transverse direction.

Model/element type	Q N	M Nm/m	$\varphi_{\max}$ degrees	$M_{\max}$ (Nm/m)
Axisymmetric solid (4 node elements)	953.7	-10.57	-	-
Axisymmetric solid (8 node elements)	953.7	-19.67	-	-
Axisymmetric shell - solid	593.8	-140.12	-	-
Axisymmetric shell - solid	-	-78.63	-	-
3D shell - solid	1140.0	-205.00	37.70	215.00
3D shell - solid	16660.0	17976.6	-	-
Axisymmetric solid	963.2	-33.73	-	-
3D shell - solid	1015.7	86.30	-	231.09
Axisymmetric shell - solid	949.2	-36.62	-	-
3D shell - solid	951.3	-38.35	-	-
Axisymmetric shell - solid	989.1	-89.11	38.00	238.63

Table 6: Summary of the challenge problem results with the h-version.

Appendix: Summary of challenge problem results

We reproduce here from [4] the results received in response to the Girkmann challenge problem. The four results based on the p-version and the eleven results based on the h-version are shown in Tables 5 and 6, respectively.

References

[1] J. Pitkäranta, I. Babuška, B. A. Szabó, The Girkmann problem, IACM Expr. 22 (2008) 28.

[2] K. Girkmann, Flächentragwerke, Springer, Wien, 1954.

[3] J. Pitkäranta, B. A. Szabó, I. Babuška, The problem of verification with reference to the Girkmann problem, IACM Expr. 24 (2009) 14–15.

[4] B. A. Szabó, I. Babuška, J. Pitkäranta, S. Nervi, The problem of verification with reference to the Girkmann problem, Engineering with Computers 26 (2010) 171–183.

[5] P. J. Roache, Fundamentals of Verification and Validation, Hermosa, New Mexico, 2009.

[6] Guide for Verification and Validation in Computational Solid Mechanics, ASME V&V 10-2006, The American Society of Mechanical Engineers, New York, 2006.

[7] I. Babuška, T. Strouboulis, The Finite Element Method and its Reliability, Oxford: Clarendon Press, United States, 2001.

[8] R. Tews, W. Rachowicz, Application of an automatic *hp* adaptive Finite Element Method for thin-walled structures, Comput. Methods Appl. Mech. Engrg. 198 (2009) 1967–1984.

[9] I. Babuška, A. Miller, The post-processing approach in the finite element method – part 1: calculation of displacements, stresses and other higher derivatives of the displacements, Int. J. Numer. Meth. Engng 20 (1984) 1085–1109.

[10] L. F. Demkowicz, Computing with *hp*-ADAPTIVE FINITE ELEMENTS: Volume 1 One and Two Dimensional Elliptic and Maxwell problems, CRC Press, United States of America, 2007.

[11] J. Pitkäranta, I. Babuška, The dome and the ring: Verification of classical back-of-the-envelope models for designing a stiffened shell roof, To appear.

[12] A. H. Niemi, Approximation of shell layers using bilinear elements on anisotropically refined rectangular meshes, Comput. Methods Appl. Mech. Engrg. 197 (2008) 3964–3975.

[13] A. H. Niemi, A bilinear shell element based on a refined shallow shell model, Int. J. Numer. Meth. Engng 81 (2010) 485–512.

[14] J. Pitkäranta, A.-M. Matache, C. Schwab, Fourier mode analysis of layers in shallow shell deformations, Comput. Methods Appl. Mech. Engrg. 190 (2001) 2943–2975.